



LAWRENCE  
LIVERMORE  
NATIONAL  
LABORATORY

# Quantification of large and localized deformation in granular materials

P. Fu, Y. F. Dafalias

April 11, 2011

International Journal of Solids and Structures

## **Disclaimer**

---

This document was prepared as an account of work sponsored by an agency of the United States government. Neither the United States government nor Lawrence Livermore National Security, LLC, nor any of their employees makes any warranty, expressed or implied, or assumes any legal liability or responsibility for the accuracy, completeness, or usefulness of any information, apparatus, product, or process disclosed, or represents that its use would not infringe privately owned rights. Reference herein to any specific commercial product, process, or service by trade name, trademark, manufacturer, or otherwise does not necessarily constitute or imply its endorsement, recommendation, or favoring by the United States government or Lawrence Livermore National Security, LLC. The views and opinions of authors expressed herein do not necessarily state or reflect those of the United States government or Lawrence Livermore National Security, LLC, and shall not be used for advertising or product endorsement purposes.

# Quantification of large and localized deformation in granular materials

Pengcheng Fu<sup>a</sup>, Yannis F. Dafalias<sup>bc</sup>

<sup>a</sup>Atmospheric, Earth, and Energy Division, Lawrence Livermore National Laboratory, 7000 East Avenue, L-286, Livermore, CA 94551, USA

Corresponding author; Email: fu4@llnl.gov; pfu@ucdavis.edu. Tel: 1-925-422-3579

<sup>b</sup>Department of Civil and Environmental Engineering, University of California, Davis, CA 95616, USA

<sup>c</sup>Department of Mechanics, School of Applied Mathematical and Physical Sciences, National Technical University of Athens, Zographou Campus, Athens, Greece

## Abstract:

Quantifying large deformation in granular assemblies using concepts originating from continuum mechanics is a challenging task because of 1) the discontinuous nature of granular displacement, which does not allow the definition of a continuum measure of deformation, and 2) the almost inevitable shear band localization. These problems exist in both real-world granular materials and their numerical idealizations using the discrete element method (DEM). In this work a new method is developed in order to address these issues. Instead of creating a meshed equivalent continuum for quantifying small engineering strains, the new method performs independent random queries on the velocity gradient characteristics of arbitrary sub-domains in the assembly through the novel concept of overlapping reference triangles, thus, enabling rigorous handling of large deformations which are usually associated with localization. The proposed method is illustrated and validated by DEM simulation of a biaxial compressive test, in which apparent shear banding takes place. The homogenized deformation quantifications based on the new method match the estimations from the imposed boundary conditions. The numerical examples are also applied to 1) quantifying the heterogeneous distribution of deformation over the specimen, 2) visualizing the nucleation process of shear bands, and 3) characterizing shear flow patterns in shear bands. An investigation on the effects of the reference triangle sizes yields some inspiring and practically significant results.

## 1. Introduction

Particle-based methods, including laboratory experiments with particle-level measurements and discrete element-type numerical simulations are important means of studying fundamental behaviors of granular materials. These methods yield particle-level quantities regarding the movements of particles and their mutual relationships (e.g. contacts and contact forces). Micromechanically based constitutive relationships can be directly established between these quantities but they are impractical to be used in solving real world engineering problems. In order to develop conventional constitutive theories in the context of continuum mechanics inspired by these particle-based methods, continuum-based variables of stress and strain measures need to be derived from particle-level quantities. Whereas formulations for calculating averaged stress tensors from inter-particle contact forces are well established, various

problems have been encountered in the effort to obtain homogenized strain measurements based on the displacement field in granular media. This difficulty can be attributed to the following two factors. First, neither granular particle assemblies themselves nor any quantities defined for particles are continuous over the domain. The homogenization of stress over a domain does not require derivatives or partial derivatives of any variable and is mainly based on contact forces. On the other hand, strain tensors are defined as partial derivatives of the displacement field, heavily relying on the continuity assumption. Second, the definition of stress does not require any “reference state” to be identified while strain is usually determined by exploring the relationships between the domain’s current state and a reference configuration.

Important progresses have been made in determining average strain tensors based on the movements of individual particles. These methods are either based on 1) an equivalent continuum (which is usually meshed) attached to the granular assembly (e.g. Bagi, 1996; Kruyt and Rothenburg, 1996; Kuhn, 1999; Cambou et al. 2000; Kruyt, 2003; Tordesillas et al. 2008; Li and Li, 2009), or 2) a best-fit approach to find the average strain tensor that minimizes the difference between the observed particle (or contact) movements and that predicted by the strain tensor (Liao, 1997; ITASCA, 1999). Thorough comparisons and evaluations of these methods have been conducted by Cambou et al. (2000), Bagi (2006), and Durán et al. (2010), and are not repeated here. It was noteworthy that among the methods in the first category, the formulations proposed by Bagi (1996), Kruyt and Rothenburg (1996), Kuhn (1997, 1999), and Cambou et al. (2000) were essentially based on the same assumptions, and they were found to yield strain estimations closely matching the values calculated based on boundary displacements applied to the granular assemblies. On the other hands, the credibility of some other methods is questionable, but this issue is not further explored in this paper. Despite these successes, several issues remain outstanding.

First, the existing methods did not pay sufficient attention to the strain localization phenomenon, or more specifically, shear banding in granular materials. It has been discovered in experimental studies utilizing advanced imaging technologies that strain localization is almost a universal phenomenon for both loose and dense sand specimens under drained as well as undrained test conditions (Finno et al. 1996, 1997). X-ray computed tomography (CT) analysis (Desrues et al. 1996) has revealed that some seemingly uniform deformation patterns are in fact the results of complex shear localization (or shear banding) patterns inside the soil specimens. Once shear banding takes place in a deforming granular specimen, deformation usually concentrates in relatively thin zones and the other portions of the specimen experience essentially rigid body displacement. Under this condition, constitutive modeling should focus on the shear bands since the physical and mechanical meaning of homogenized variables over the entire specimens is ambiguous. This is especially important if shear bands in the same material but forming under different boundary conditions are to be analyzed (Fu and Dafalias, 2011b) in order to yield unified constitutive models. However, studies focusing on strains or other deformation characteristics calculated within the shear bands have been scarce in the literature.

Second, all the existing methods are based on the engineering strain (i.e. the infinitesimal strain tensor, sometimes termed the Cauchy strain tensor), which is only appropriate for small deformation problems. Even if the homogenized deformation over the entire specimen is considered small, the shear deformation in the predominant shear bands is so large that the infinitesimal strain theory loses legitimacy.

Third, many of the existing methods are only applicable to assemblies of convex particles. This is because most of these methods require tessellating the analysis domain with triangles (Bagi, 1996), polygons (Kruyt and Rothenburg, 1996), or polyhedrons, and many of the tessellation algorithms are only applicable to convex particle shapes.

In this paper, we develop, validate and demonstrate a new method for quantifying deformation characteristics in granular assemblies, with special consideration for **strain localization** (especially shear banding) and **large deformation**. The equivalent continuum quantities of interest are the velocity gradient tensor, a natural consequence of the finite character and the flow type of deformation predominant in granular assemblies under large shear. The formulations are developed and the concept of reference triangles is defined in Section 2 of the paper. In Section 3 and Section 4, the effectiveness of the proposed method is demonstrated through detailed analysis of the deformation evolution in a virtual (DEM) biaxial compression specimen with apparent shear banding development. In Section 5, the effects of an important parameter, the size of the reference triangles, on the quantified deformation measurements, is evaluated.

## 2. Method Development

### *2.1 Basic premises and outline of the new method*

The new method is developed based on the following theoretical considerations and assumptions.

Instead of employing the commonly used engineering strains, the new method is based on the velocity gradient tensor. The theoretical concepts and numerical implementation are elaborated in Sections 2.2 and 2.3, respectively. This framework enables rigorous handling of large deformation problems. Individual components of the velocity gradient tensor can be integrated under certain circumstances to obtain physically meaningful metrics for quantifying large deformation of a given domain. These metrics can be related to conventionally used quantities as described in Section 2.5.

The new method calculates the deformation rate on individual sub-domains in the granular assembly with the help of reference triangles, so the conventional method of attaching a virtual continuum to the assembly and discretizing this continuum into meshes is avoided. Since the sub-domains are independent of each other and so are the reference triangles, the calculation based on each reference triangle is essentially an independent query, making random sampling and statistical interpretations of results convenient.

The development of the new method is carried out in a two-dimensional (2D) space and demonstrated through 2D numerical examples. However, all the formulations can be easily extended to a 3D space as will be briefly discussed in Section 2.6.

### *2.2 Velocity gradient tensor, rate-of-deformation tensor, and spin tensor*

At a given moment  $t$  in a continuum, the velocity field is  $\mathbf{v}(\mathbf{x}, t)$  or  $v_i(x_1, x_2, t)$ ,  $i=1, 2$ , where  $x_1$  and  $x_2$  (or  $\mathbf{x}$  in the vector format) represent the location of any point in a 2D continuum. The velocity gradient tensor  $\mathbf{L}$  is given by

$$\mathbf{L} = [L_{ij}] = [v_{i,j}] = \begin{bmatrix} v_{1,1} & v_{1,2} \\ v_{2,1} & v_{2,2} \end{bmatrix} = \begin{bmatrix} \partial v_1 / \partial x_1 & \partial v_1 / \partial x_2 \\ \partial v_2 / \partial x_1 & \partial v_2 / \partial x_2 \end{bmatrix} \quad (1)$$

Tensor  $\mathbf{L}$  can be written as the sum of a symmetric tensor  $\mathbf{D}$  and a skew-symmetric tensor  $\mathbf{W}$  (i.e.  $\mathbf{L} = \mathbf{D} + \mathbf{W}$ ), termed the rate-of-deformation tensor and the spin tensor, respectively, and given by

$$\mathbf{D} = [D_{ij}] = \left[ \frac{1}{2} (v_{i,j} + v_{j,i}) \right] = \begin{bmatrix} v_{1,1} & (v_{1,2} + v_{2,1})/2 \\ (v_{1,2} + v_{2,1})/2 & v_{2,2} \end{bmatrix} \quad (2)$$

$$\mathbf{W} = [W_{ij}] = \left[ \frac{1}{2} (v_{i,j} - v_{j,i}) \right] = \begin{bmatrix} 0 & (v_{1,2} - v_{2,1})/2 \\ -(v_{1,2} - v_{2,1})/2 & 0 \end{bmatrix} \quad (3)$$

To demonstrate the physical significance of these tensors, we can consider two points  $p$  and  $q$  in the continuum connected by an infinitesimal vector  $d\mathbf{x}^{pq} = \mathbf{x}^q - \mathbf{x}^p$  pointing from  $p$  to  $q$ . The velocity at  $q$  relative to that at  $p$  is  $d\mathbf{v}^{pq} = \mathbf{L}d\mathbf{x}^{pq} = \mathbf{D}d\mathbf{x}^{pq} + \mathbf{W}d\mathbf{x}^{pq}$ , where  $\mathbf{D}d\mathbf{x}^{pq}$  represents the contribution from the deformation rate of the continuum near  $p$  and  $\mathbf{W}d\mathbf{x}^{pq}$  represents the contribution from the rate of rigid body rotation near  $p$ .

### 2.3 Numerical evaluation of velocity gradient tensors and the concept of reference triangles

The following two facts should be considered and exploited in order to develop numerical formulations for calculating the velocity gradient in a granular assembly.

- 1) A deforming granular assembly can only be considered as a continuum in an approximately sense. Velocity is not defined for voids and it is not continuous across inter-particle contact points where sliding and rolling is taking place.
- 2) The overall inelastic deformation of a granular assembly is mainly attributed to the relative displacements of individual particles, whereas the internal deformation of individual particle bodies can be ignored for most applications. Therefore, both the velocity gradient tensor and the more conventional small strain tensor can only be meaningfully defined for domains consisting of multiple particles.

Figure 1 shows a sub-domain in a granular assembly consisting of a few dozen arbitrarily shaped particles. A reference triangle is identified with its three vertices attached to and moving with the centers of three reference particles. If we assume that 1) the velocity field in this triangular domain varies linearly over the triangular area, and 2) the centers of other particles within this triangular domain have approximately the same velocities as the velocities of the corresponding points in the triangle, then the homogenized velocity gradient tensor can be calculated following the procedure below.

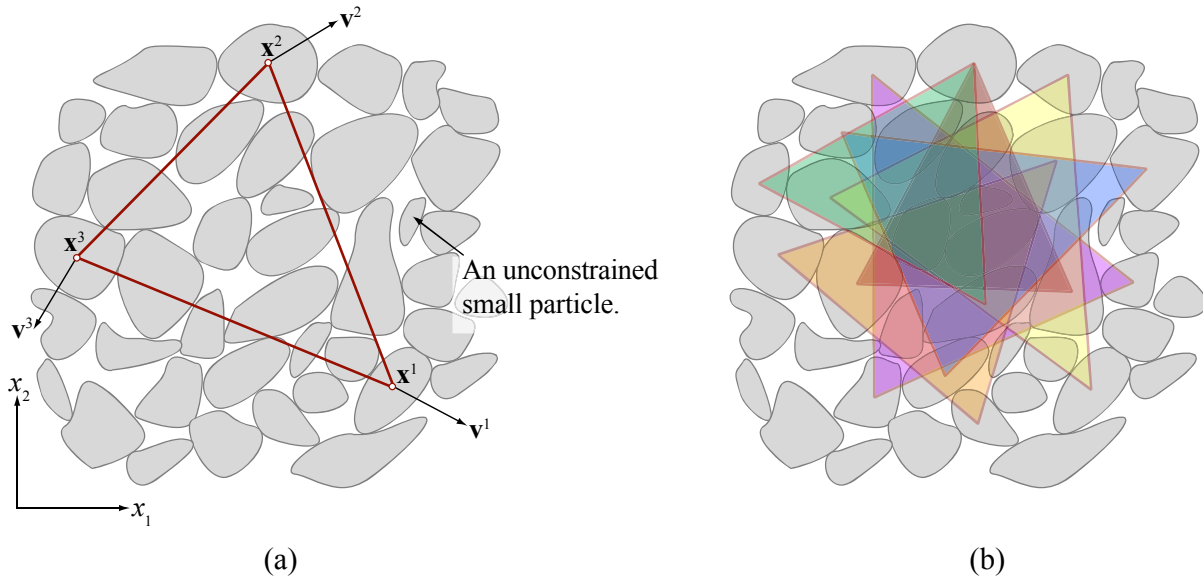


Figure 1 Reference triangle for a sub-domain in a granular assembly. (a) Locations and velocities of the three reference particles, and (b) multiple overlapping reference triangles constructed for the same sub-domain.

We need to establish first a parametric coordinate system (also termed the triangular coordinates, or natural coordinates) as shown in Figure 2. The location of any point inside the triangle relative to the three vertices can be expressed by three parameters  $\zeta_1$ ,  $\zeta_2$ , and  $\zeta_3$ .  $\zeta_1 = l_1/L_1$ , where  $l_1$  and  $L_1$  are the distance from this point and corner  $\mathbf{x}^1$  to side  $\mathbf{x}^2\mathbf{x}^3$ , respectively, and  $\zeta_2$  and  $\zeta_3$  can be defined in a similarly fashion. Only two of these three parameters are independent as  $\zeta_1 + \zeta_2 + \zeta_3 = 1$ . The location of any point in the triangle can be expressed as linear combination of the locations of the three reference particles at the vertices according to  $\mathbf{x}(\zeta_1, \zeta_2, \zeta_3) = \zeta_1 \mathbf{x}^1 + \zeta_2 \mathbf{x}^2 + \zeta_3 \mathbf{x}^3$ , and so is its velocity as

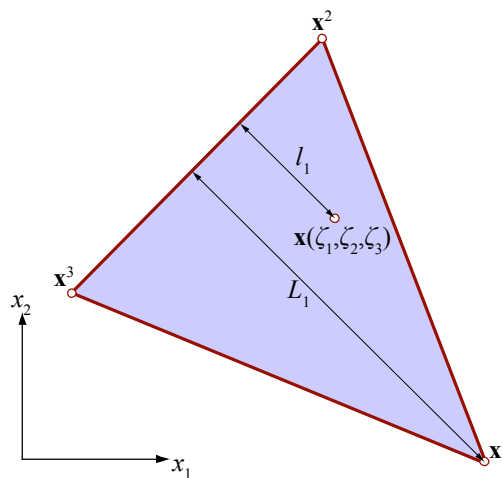


Figure 2 The triangular coordinate system.

$$\begin{bmatrix} v_1 \\ v_2 \end{bmatrix} = \begin{bmatrix} \zeta_1 & 0 & \zeta_2 & 0 & \zeta_3 & 0 \\ 0 & \zeta_1 & 0 & \zeta_2 & 0 & \zeta_3 \end{bmatrix} \begin{bmatrix} v_1^1 & v_2^1 & v_1^2 & v_2^2 & v_1^3 & v_2^3 \end{bmatrix}^T \quad (4)$$

The four components of tensor  $\mathbf{L}$  can be calculated according to

$$\begin{aligned} \begin{bmatrix} v_{1,1} \\ v_{1,2} \\ v_{2,1} \\ v_{2,2} \end{bmatrix} &= \begin{bmatrix} \partial/\partial x_1 & 0 \\ \partial/\partial x_2 & 0 \\ 0 & \partial/\partial x_1 \\ 0 & \partial/\partial x_2 \end{bmatrix} \begin{bmatrix} v_1 \\ v_2 \end{bmatrix} \\ &= \begin{bmatrix} \zeta_{1,1} & 0 & \zeta_{2,1} & 0 & \zeta_{3,1} & 0 \\ \zeta_{1,2} & 0 & \zeta_{2,2} & 0 & \zeta_{3,2} & 0 \\ 0 & \zeta_{1,1} & 0 & \zeta_{2,1} & 0 & \zeta_{3,1} \\ 0 & \zeta_{1,2} & 0 & \zeta_{2,2} & 0 & \zeta_{3,2} \end{bmatrix} \begin{bmatrix} v_1^1 & v_2^1 & v_1^2 & v_2^2 & v_1^3 & v_2^3 \end{bmatrix}^T \\ &= \frac{1}{2A} \begin{bmatrix} x_2^2 - x_2^3 & 0 & x_2^3 - x_2^1 & 0 & x_2^1 - x_2^2 & 0 \\ x_1^3 - x_1^2 & 0 & x_1^2 - x_1^3 & 0 & x_1^1 - x_1^2 & 0 \\ 0 & x_2^2 - x_2^3 & 0 & x_2^3 - x_2^1 & 0 & x_2^1 - x_2^2 \\ 0 & x_1^3 - x_1^2 & 0 & x_1^2 - x_1^3 & 0 & x_1^1 - x_1^2 \end{bmatrix} \begin{bmatrix} v_1^1 & v_2^1 & v_1^2 & v_2^2 & v_1^3 & v_2^3 \end{bmatrix}^T \end{aligned} \quad (5)$$

where the derivation utilizes the following relationships

$$\zeta_{i,1} = \partial \zeta_i / \partial x_1 = \frac{1}{2A} (x_2^j - x_2^k), \text{ and } \partial \zeta_i = \partial \zeta_i / \partial x_j = \frac{1}{2A} (x_1^k - x_1^j) \quad (6)$$

with  $j$  and  $k$  denoting the 3-cyclic permutations of  $i$ , and  $A$  is the area of this triangle. Once tensor  $\mathbf{L}$  is calculated, the rate-of-deformation tensor  $\mathbf{D}$  and the spin tensor  $\mathbf{W}$  can be obtained using equations (2) and (3), respectively. If information about velocities of individual particles is unavailable but particle locations are known at a series of time instances, the following central-difference formulation can be used to estimate  $\mathbf{L}$ , which is potentially more desirable because measurements of locations are less volatile than those for velocities in a deforming granular assembly.

$$\begin{bmatrix} v_{1,1} \\ v_{1,2} \\ v_{2,1} \\ v_{2,2} \end{bmatrix}_{t+dt/2} = \frac{1}{2Adt} \begin{bmatrix} x_2^2 - x_2^3 & 0 & x_2^3 - x_2^1 & 0 & x_2^1 - x_2^2 & 0 \\ x_1^3 - x_1^2 & 0 & x_1^2 - x_1^3 & 0 & x_1^1 - x_1^2 & 0 \\ 0 & x_2^2 - x_2^3 & 0 & x_2^3 - x_2^1 & 0 & x_2^1 - x_2^2 \\ 0 & x_1^3 - x_1^2 & 0 & x_1^2 - x_1^3 & 0 & x_1^1 - x_1^2 \end{bmatrix}_{t+\frac{dt}{2}} \begin{bmatrix} x_1^1(t+d) - x_1^1(t) \\ x_2^1(t+d) - x_2^1(t) \\ x_1^2(t+d) - x_1^2(t) \\ x_2^2(t+d) - x_2^2(t) \\ x_1^3(t+d) - x_1^3(t) \\ x_2^3(t+d) - x_2^3(t) \end{bmatrix} \quad (7)$$

These tensors ( $\mathbf{L}$ ,  $\mathbf{D}$ , and  $\mathbf{W}$ ) are only functions of the current locations and velocities of the three reference particles at the vertices of the triangle, and one set of values can be computed for a selected reference triangle. For a given sub-domain, multiple reference triangles can be constructed as shown in Figure 1(b) and therefore multiple values of  $\mathbf{L}$  (as well as the corresponding  $\mathbf{D}$  and  $\mathbf{W}$ ) can be obtained. Moreover, rather than measuring features of the exact triangular area, the obtained values for each reference triangle reflect deformation rate characteristics of the particles in this “neighborhood” without a

clear-cut boundary. This ambiguity in fact reflects the very nature of a deforming granular assembly: any variable quantifying its deformation (as well as deformation rates) on the basis of analogy to continuum mechanics can only be approximately determined, i.e. no exact and unique strain or rate-of-deformation is defined for granular materials. Calculations based on these overlapping reference triangles can be considered as random “queries” on the rate of deformation features of this domain. Basic principles of statistics are well reflected: the more uniform the deformation pattern, the smaller variance among the individually queried values one can expect. The average value of these individual queries should provide a reliable quantification of the overall rate of deformation characteristics in this domain.

Practically, reference triangles with approximately equal edge lengths (i.e. close to equilateral triangles) are preferred to minimize numeric errors, based on the same considerations why equilateral triangle elements are preferred in finite element analysis. Another practical consideration for selecting particles to which the reference triangles are attached is that it is desired to use relatively large particles. Smaller particles are more likely to be kinematically “unconstrained”, i.e. it can freely move to some extent in voids between relative large particles, as shown in the example in Figure 1(a). Therefore, the velocity and displacement of such small particles is not very meaningful in terms of representing the deformation characteristics of the stress-wise active part of the assembly, since constrained rather than “free” contacts are necessary to create forces contributing to the stress definition. If such small particles are used to construct the reference triangles, the obtained deformation rate values will have a rather high chance to be “noises” instead of meaningful measurements. This phenomenon will be further investigated in Section 5 where we evaluate the effects of reference triangle sizes.

When a reference triangle deforms with the granular assembly, its shape can gradually become skewed or even flipped with a numerically negative area. However, this is not an issue for the proposed method because the determination of tensors  $\mathbf{L}$ ,  $\mathbf{D}$  and  $\mathbf{W}$  only requires information of the current state of the domain and do not rely on a fixed previous “reference configuration” of the particles. Therefore, over any period of time, a reference triangle for a given sub-domain does not have to be attached to the same reference particles, and it can be freely replaced anytime by one which is attached to three different reference particles for the next increment. Moreover, because the reference triangles can be constructed freely, this method is applicable to both convex and concave particle shapes.

The triangular “space cell” system proposed by Bagi (1996) or the Delaunay triangles constructed based on the particle centers can be seen as the smallest reference triangles that can be adopted for a granular assembly. Two distinct features differentiate the new method from the existing methods. First, the new method is based on the rate-of-deformation concept capable of handling large deformation problems whereas most existing methods are based on the small strain tensor for small deformation problems. Second, the sizes of the reference triangles of our method can be flexibly selected according to the needs of the problem to be studied while the tessellation system used by the existing methods is almost fixed for a given particle assembly. For instance, the thicknesses of shear bands have been typically reported to be 8 to 20 times the mean sand particle sizes, also depending on some other factors (Mühlhaus and Vardoulakis, 1987; Oda and Kazama, 1998; Alshibli and Sture, 1999). In order to study deformation features inside shear bands, reference triangles with edge lengths four to six times of mean particle diameters should provide sufficient resolution. It is rare to encounter cases where deformation features at

length scales similar to particle sizes are concerned. Nevertheless, reference triangles constructed using the Delaunay triangulation represent the lower limit of reference triangle sizes and will be used to study the effects of reference triangle sizes in Section 5.

#### 2.4 Local shear flow rate and the shear flow direction

Shear banding is the most important strain localization phenomenon in granular materials. Not only is it observed in laboratory tests, but it also takes place in the field as shear failures of foundations and slopes are usually accompanied by shear banding. The initiation and development of shear bands in a granular assembly with a relatively homogeneous initial state is a rather complex process, as revealed by modern imaging techniques (Desrues and Viggiani, 2004; Rechenmacher, 2006). Since the deformation mode of a “mature” shear band (deforming in its ultimate steady state) is more or less analogous to laminar flow of fluids, it is natural to assume that this shear-type grain flow plays a critical role in the development of shear bands. To study the shear banding phenomenon requires quantifying and tracking this type of shear flow in granular assemblies throughout the entire deformation process. Consider a small neighborhood of granular particles with known arbitrary velocity field  $\mathbf{v}(\mathbf{x})$  as shown in Figure 3, for which the  $\mathbf{L}$ ,  $\mathbf{D}$ , and  $\mathbf{W}$  tensors have been calculated using the method described above. The current section aims at developing appropriate methods to 1) identify the shear flow direction from  $\mathbf{L}$ ,  $\mathbf{D}$ , and  $\mathbf{W}$ , and 2) quantify the shear flow rate. Although the velocity field shown in Figure 3 to some extent resembles a laminar flow, the method to be developed in this section is applicable to arbitrary velocity fields. In a mature shear band experiencing steady flow, the local shear flow direction should be the same as the overall orientation of the shear band (which itself has attracted substantial interest, e.g. Vermeer, 1990), but the shear flow direction, especially its distribution over the entire sample is not apparent before the mature and dominant shear band fully forms. Therefore, the method to be developed in this section is an important tool for studying the entire shear banding process starting from relatively homogeneous initial states.

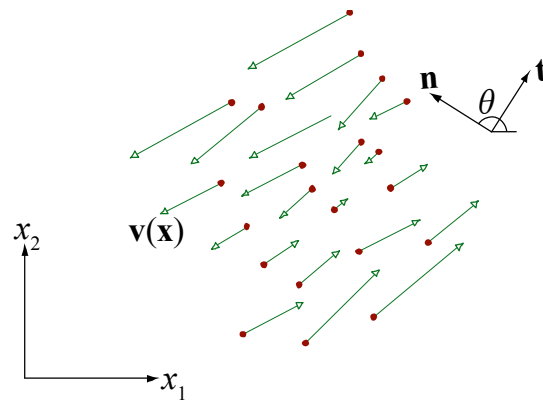


Figure 3 A small neighborhood of particles showing deformation pattern analogous to laminar flow. Only the centroids of the particles are denoted as dots but the particles are not shown.  $\mathbf{v}(\mathbf{x})$  is the velocity vector of the particle whose centroid is located at  $\mathbf{x}$ .

By making an analogue between the rate-of-deformation tensor and the small strain tensor, one might naturally postulate that the shear flow direction corresponds to the maximum shear strain direction. However, the small strain tensor yields two maximum shear strain directions orthogonal to each other,

whereas there is usually only one shear flow direction, especially in the laminar-flow type deformation pattern. It is necessary to find an unambiguous way to identify which one of the two maximum shear directions corresponds to the shear flow direction.

Consider an arbitrary reference plane with the normal and tangential directions denoted by two orthogonal unit vectors  $\mathbf{n}=(\cos\theta, \sin\theta)^T$  and  $\mathbf{t}=(\sin\theta, -\cos\theta)^T$ , respectively, where  $\theta$  (between  $0^\circ$  and  $180^\circ$ ) is the orientation angle of the normal direction measured counterclockwise from the  $x_1$  direction. The tangential velocity of the particles along this plane is  $\mathbf{v}\cdot\mathbf{t}$ , and the *local shear flow rate*  $\dot{\gamma}$  along this plane is defined as the directional derivative of the tangential velocity with respect to  $\mathbf{n}$ , namely

$$\dot{\gamma}(\theta) = \nabla_{\mathbf{n}}(\mathbf{v}\cdot\mathbf{t}) = \mathbf{L}\mathbf{n}\cdot\mathbf{t} = \frac{1}{2}(v_{1,2} - v_{2,1}) + \frac{1}{2}(v_{1,1} - v_{2,2})\sin 2\theta - \frac{1}{2}(v_{1,2} + v_{2,1})\cos 2\theta \quad (8)$$

where use of the relations  $\partial\mathbf{v}/\partial\mathbf{n} = (\partial\mathbf{v}/\partial\mathbf{x})\partial\mathbf{x}/\partial\mathbf{n} \Rightarrow \mathbf{L}\partial\mathbf{x}/\partial\mathbf{n}$  and  $\partial\mathbf{x}/\partial\mathbf{n} = \mathbf{n}$  was made in deriving this equation.

Since  $\mathbf{L}=\mathbf{W}+\mathbf{D}$ , the first term  $(v_{1,2}-v_{2,1})/2$ , a constant independent of  $\theta$  in equation (8), is induced by  $\mathbf{W}$  while the other two terms by  $\mathbf{D}$ . We define the *local shear flow direction* to be along the reference plane ( $\theta=\theta_{MaxShear}$ ) that maximizes the absolute value of  $\dot{\gamma}$ . Based on basic trigonometry, we can find out that the normal direction of the reference plane that maximize the absolute shear flow rate is given by

$$\theta_{MaxShear} = \begin{cases} \alpha/2 + \pi/4, & \text{if } v_{1,1} \geq v_{2,1} \\ \alpha/2 - \pi/4, & \text{if } v_{1,1} < v_{2,1} \end{cases} \quad (9)$$

where  $\alpha$  satisfies

$$\cos\alpha = \frac{v_{1,1} - v_{2,2}}{[(v_{1,1} - v_{2,2})^2 + (v_{1,2} + v_{2,1})^2]^{1/2}} \quad \text{and} \quad \sin\alpha = \frac{v_{1,2} + v_{2,1}}{[(v_{1,1} - v_{2,2})^2 + (v_{1,2} + v_{2,1})^2]^{1/2}} \quad (10)$$

The two angles,  $\alpha/2-\pi/4$  and  $\alpha/2+\pi/4$ , each orienting  $\pi/4$  ( $45^\circ$ ) from the principal strain directions, are the two “maximum shear” directions of the rate-of-deformation tensor  $\mathbf{D}$ . This is consistent with our “speculation” at the beginning of the section, but equation (9) reveals that it is the spin direction (or  $\mathbf{W}$ ), or equivalently its sign, that determines which one of these two orthogonal directions is also the shear flow direction.

The *maximum local shear flow rate*, namely the shear flow rate along the shear flow direction  $\theta_{MaxShear}$ , is, therefore, the absolute value of equation (8) with equations (9) and (10) plugged in as

$$\dot{\gamma}_{max} = \frac{1}{2}[(v_{1,1} - v_{2,2})^2 + (v_{1,2} + v_{2,1})^2]^{1/2} + \frac{1}{2}|v_{2,1} - v_{1,2}| \quad (11)$$

which is a positive scalar because only the absolute value of the shear flow rate is concerned in this context. However, the sign of the shear flow rate can be naturally defined if necessary, by specifying the positive direction of the tangential direction for the reference plane.

To demonstrate the meanings of the quantities defined above, we assume that the particles in an idealized shear band form a laminar flow pattern as shown in Figure 4. This special flow pattern is not necessarily realistic, but we make this assumption for illustration purposes. The normal of the shear band is oriented in the angle  $\beta$ , which here is a known quantity while  $\theta$  in Figure 3 is a variable. If the origin of the coordinate system is placed somewhere along the streamline with zero velocity, then the velocity field of the domain can be analytically described as

$$v_1 = \lambda(x_1 \cos \beta - x_2 \sin \beta) \sin \beta \quad (12)$$

$$v_2 = -\lambda(x_1 \cos \beta - x_2 \sin \beta) \cos \beta \quad (13)$$

where  $\lambda = \partial v_t / \partial n$ , is the directional derivative of the tangential velocity along the streamline direction with respect to the normal to the shear band direction. Its physical meaning is: if the lateral distance between a streamline and the neutral streamline (where  $\mathbf{v}=\mathbf{0}$ ) is  $l$ , then the tangential velocity of particles along this streamline is  $l\lambda$ .

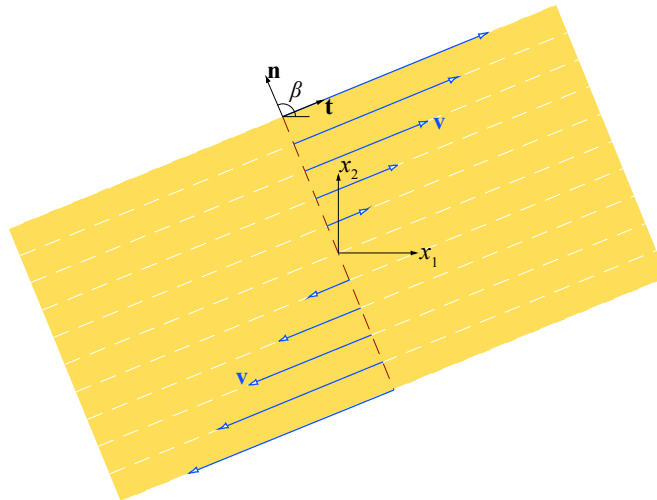


Figure 4 Flow field in an idealized shear band.

By plugging equations (12) and (13) into equations (1), (9), (10), and (11), and assuming  $\lambda > 0$ , we get shear flow direction  $\theta_{MaxShear} = \beta$  and the maximum shear flow rate  $\dot{\gamma}_{max} = \lambda$ , matching the assumed geometrical configuration. In this special configuration, the first term in equation (8) and the other two terms combined, each contribute  $\lambda/2$  to the maximum shear flow rate  $\dot{\gamma}_{max}$ . By analogy between the rate-of-deformation tensor and the small strain tensor, the maximum shear flow rate  $\dot{\gamma}_{max}$  corresponds to the maximum engineering shear strain for this assumed special velocity field (or deformation pattern), but is not necessarily true for an arbitrary velocity field.

## 2.5 Use integrals of the rate-of-deformation to quantify total deformation

The rate-of-deformation tensor is a useful concept by itself since it can be directly used in constitutive models such as those in the theories of plasticity and viscoplasticity. However, it is often desired to quantify the “total deformation” of a granular assembly or its sub-domains over a given period of time. In

fact, the current study was directly motivated by a previous investigation (Fu and Dafalias, 2011b) of the anisotropic fabric evolution in shear bands, which requires quantifying the shear deformation within shear bands that have formed under different boundary conditions.

A natural solution is to integrate the components of tensor  $\mathbf{L}$  or  $\mathbf{D}$  over this period of time. The integral of a normal component of  $\mathbf{D}$  constitutes the natural strain in this direction, such as  $\varepsilon_1^N = \int D_{11} dt$  where the superscript “ $N$ ” denotes “Natural”, as long as this direction is a fixed principal direction of  $\mathbf{D}$ , since the integration must be carried over the same material line element, i.e. following the same material points. Otherwise the integration has no meaning as a strain measure, but simply becomes a measure of deformation along a certain direction not necessarily associated with the same material points. The natural strain has the following relationship with the corresponding engineering (small) strain component  $\varepsilon_i^E = \ln \left( \frac{d_i}{d_i^E} \right)$ , where the superscript “ $E$ ” denotes “Engineering” (also termed the “Cauchy strain”). This relationship provides a useful means to relate the method proposed in this paper to the more conventionally used engineering strain. The time integration of the normal components of  $\mathbf{D}$  can also be used to track the evolution of void ratio  $e$  as.

$$\ln \left[ \frac{1+e(t)}{1+e(0)} \right] = \int_0^t v_{1,1} + v_{2,2} dt \quad (14)$$

where  $e(0)$  and  $e(t)$  are the void ratios at the reference state the current state, respectively. The term  $v_{1,1}+v_{2,2}$  can be considered an analogue to the volumetric strain  $\varepsilon_V = \varepsilon_{11} + \varepsilon_{22}$  in small deformation problems. Notice that Eq.(14) does not require the fixing of the principal directions of  $\mathbf{D}$ , since the  $v_{1,1}+v_{2,2}$  measures rate of volume and is invariant (a trace) in regards to the choice of axes 1 and 2.

Time integration can be conducted on the shear component  $D_{12}$  in a similar fashion, and such an integral might provide a useful metric for material shear deformation, not necessarily a strain tensor component, but this is not pursued in the current paper. Instead, we use  $\gamma_{max} = \int \dot{\gamma}_{max} dt$  to measure the total shear deformation (but not shear strain tensor) that has taken place in any small domain from a reference state. Note that the value of  $\gamma_{max}$  is independent of the choice of coordinate system  $x_1-x_2$ , whereas  $D_{12}$  is dependent on the orientation of the coordinate system. In general, although  $\mathbf{D}$  itself is a Cartesian tensor, the integrals of  $D_{ij}$  do not constitute a Cartesian tensor, even more a strain tensor. We only use these integrals as physically meaningful metrics for overall deformations in a granular assembly.

If what has been obtained from particle-based numerical simulations or experiments are discrete measurements at a series of states of the assembly instead of continuous functions of the time, the aforementioned time integrations can be converted into a summation format utilizing these discrete measurements, namely

$$\int v_{i,j} dt \approx \sum d_j t \quad (15)$$

where  $v_{i,j} dt$  can be easily obtained by rearranging the central difference formulation in equation (7) as

$$\begin{bmatrix} v_{1,1} dt \\ v_{1,2} dt \\ v_{2,1} dt \\ v_{2,2} dt \end{bmatrix} = \frac{1}{2A} \begin{bmatrix} x_2^2 - x_2^3 & 0 & x_2^3 - x_2^1 & 0 & x_2^1 - x_2^2 & 0 \\ x_1^3 - x_1^2 & 0 & x_1^1 - x_1^3 & 0 & x_1^2 - x_1^1 & 0 \\ 0 & x_2^2 - x_2^3 & 0 & x_2^3 - x_2^1 & 0 & x_2^1 - x_2^2 \\ 0 & x_1^3 - x_1^2 & 0 & x_1^1 - x_1^3 & 0 & x_1^2 - x_1^1 \end{bmatrix} \Big|_{t+\frac{dt}{2}} \begin{bmatrix} x_1^1(t+d) - x_1^1(t) \\ x_2^1(t+d) - x_2^1(t) \\ x_1^2(t+d) - x_1^2(t) \\ x_2^2(t+d) - x_2^2(t) \\ x_1^3(t+d) - x_1^3(t) \\ x_2^3(t+d) - x_2^3(t) \end{bmatrix} \quad (16)$$

### 2.6 Extension to three-dimension

The aforementioned development in 2D can be readily extended to three-dimensional formulations if particle level quantities in 3D are to be analyzed. Such 3D data can be either simulation results of 3D DEM or from advanced imaging technologies (e.g. Hall et al. 2010; Hasan and Alshibli, 2010) applied to laboratory testing of granular materials. The 3D counterpart of the 2D reference triangles are tetrahedrons with its four vertices attaching to four particles. We notice that the format of equation (5) is somewhat similar to the equation used to calculate strains in three-node triangle finite element (the Turner triangle), so the equation for calculating the  $\mathbf{L}$  tensor (3x3) in 3D can be derived based on an analogy to the four-node tetrahedral finite element. The detailed formulations are not provided in this paper. The plane of the shear band (or the plane of maximum shear flow rate) is perpendicular to the plane constituted by the first and third principal directions of tensor  $\mathbf{D}$ .

### 3. Numerical example I: analyzing $D_{22}$ in a compression test

In this section, we apply the proposed method to a biaxial compression test to demonstrate its use in quantifying overall behaviors of the specimen. The test results are based on DEM simulation of idealized virtual particles, but extension of the method to 2D laboratory experimental data is straightforward.

#### 3.1 Brief description of the discrete element model

The DEM model consists of ellipse-shaped virtual particles simulated using the polyarc element (Fu et al., 2011c). All the particles have the same aspect ratio of 1/3. If we use the minor axis length to represent the size of a particle, the particle diameters are between 0.1 mm and 0.33 mm with a random and continuous distribution, with the mean particle size  $d_{50}=0.24$  mm and the uniformity coefficient  $d_{60}/d_{10}=2.16$ . The inter-particle friction angle used in the simulation is 35 degrees. The virtual specimen consists of 45,000 particles and is approximately 100 mm tall and 50 mm wide in its undeformed initial state. The boundary conditions applied in this simulation resemble a real world plain strain biaxial compression test as shown Figure 5. A constant confining pressure of 100 kPa is applied to the left and right boundaries and the compression in the vertical direction is applied through two rigid platens moving inward at a constant rate  $v_{bc}$ . Since particles at the left and right boundaries are dynamically and automatically detected, the confining pressure boundary condition is flexible as shown in the magnified view in Figure 5. Additionally, the two loading platens are free to move in the horizontal direction. These two conditions allow shear banding to develop with little kinematic constrains. The average initial particle orientation in this simulation is horizontal. A large number of similar biaxial compression simulations with a wide spectrum of initial fabrics have been thoroughly analyzed and reported in our previous studies (Fu and

Dafalias 2011a, 2011b), so the DEM model itself and the parameters are not further described in the current paper.

The loading of this specimen is slow enough to be considered quasi-static. For quasi-static deformation where the inertial effects can be ignored, the absolute values of the loading rate and rate-of-deformation are of a minimal significance. Consequently, the “time” used in all the analysis below is a *virtual time* so that all the “rate” quantities are normalized. The “virtual second” is selected in such a way to make  $v_{bc} \times 1$  virtual second =  $0.05H_0$ , where  $H_0$  is the initial height of specimen. Therefore, this virtual time system is closely tied to the axial deformation of the specimen. For instance, at 1 and 2 virtual seconds after the loading has commenced, the specimen should have vertical (engineering) strains of -10% and -20% (engineering strain), respectively. Note that both the upper and lower platens move at the same rate and we consider compressive strain to be negative in order to be consistent with the rate-of-deformation definition.

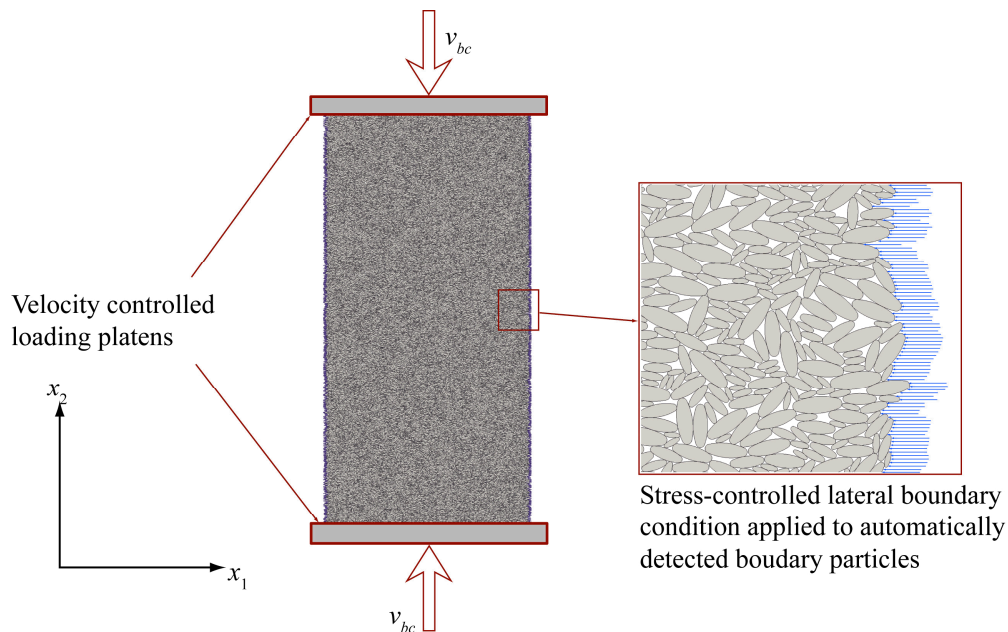


Figure 5 Boundary condition for the biaxial compression simulation.

### 3.2 General observations on mechanical responses

The evolution of stress ratio  $\sigma_{22}/\sigma_{11}$  and volumetric strain  $\varepsilon_v$  is shown in Figure 6, where  $\sigma_{11}$  and  $\sigma_{22}$  are the normal stress components in the  $x_1$  and  $x_2$  directions, respectively. In this particular case they happen to be the two principal stress components. The simulation results are typical of dense sand behaviors: the stress ratio first increases to a peak and then declines and approaches a steady value; the volumetric strain briefly decreases (representing shrinking volume) before significant dilation takes place and eventually the steady state (critical state) volume is reached. Eight representative reference states from ① to ⑧ are labeled in Figure 6: ① is the initial undeformed state; ② represents the elastic regime; in states ③ to ⑤ both the stress ratio and the dilation rate are around their peak values; the stress ratio is declining in

state ⑥ from its peak to the steady state; and both state ⑦ and state ⑧ are in the steady state with axial strains of -10% and -15% respectively. The overall deformation patterns in six of the eight states are shown in Figure 7, where all the particles are “dyed” into white and black colors to form a regular grid in the initial state. In states ② to ⑤, axial compression and lateral expansion can hardly be observed. The initiation of a shear band is merely visible in state ⑥, but this shear band clearly dominates the deformation in states ⑦ and ⑧.

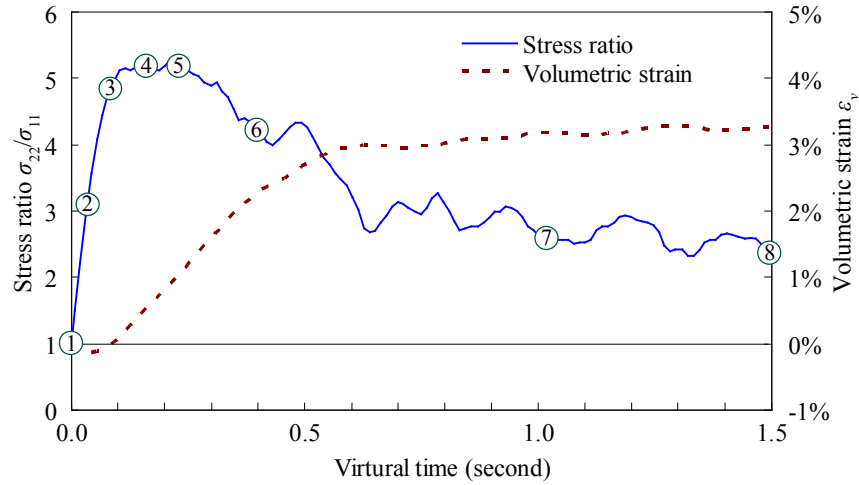


Figure 6 Evolution of the stress ratio and volumetric strain. Note the interchangeability of the virtual time and axial compressive strain: 1 virtual second is equivalent to 10% of compressive (engineering) strain.

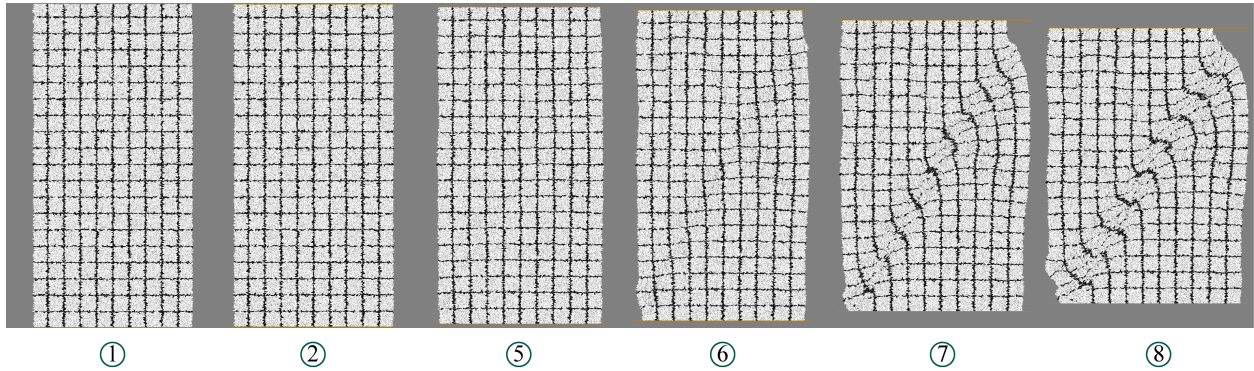


Figure 7 Overall deformation pattern of the specimen in six reference states.

### 3.3 Compare results of the proposed method with estimations based on the boundary condition

Even though the deformation of the specimen is highly non-uniform due to the development of the shear band, the average value of  $D_{22}$  can be estimated according to applied boundary condition. Since the virtual time system is selected in a way to make  $2v_{bc}=0.1H_0$ , we can derive how  $D_{22}$  evolves with time as

$$\bar{D}_{22}(t) = -\frac{2v_{bc}}{H(t)} = -\frac{2v_{bc}}{H_0(1-0.1t)} = -\frac{1}{10-t} \quad (17)$$

where  $H(t)$  is the specimen height at time  $t$ , and the bar symbol “-” over  $D_{22}$  indicates that this variable is

an average over the entire specimen. According to equation (17), the absolute value of  $\bar{D}_{22}$  increases as the specimen becomes shorter.

An alternative method for estimating  $\bar{D}_{22}$  is to randomly assess numerous sub-domains of this specimen using the method proposed in this paper and evaluate statistical characteristics of the  $D_{22}$  values obtained from these sub-domains. To this end we create approximately 3,000 reference triangles randomly distributed over the specimen. The average edge length of these triangles is 4mm, and the total area is approximately 20,000 mm<sup>2</sup>, four times of the cross section area of the specimen itself due to the significant overlapping of the reference triangles.  $D_{22}$  is calculated for each sub-domain at virtual time intervals of 0.1 second throughout the simulation. As shown in Figure 7, the shape of the specimen becomes severely distorted at large deformation, similar to typical triaxial and biaxial tests in the real world. The portions that have bulged out are not sufficiently constrained by the upper and lower loading platens, and therefore  $D_{22}$  in these portions might not be consistent with what is predicted by equation (17) based on the boundary movement. Consequently, the middle portion of the specimen that is less affected by the irregular boundary shape is identified within a white frame as shown in Figure 8(a). Average values and standard deviations of  $D_{22}$  are calculated for both the entire specimen and the middle portion only and plotted in Figure 8(b).

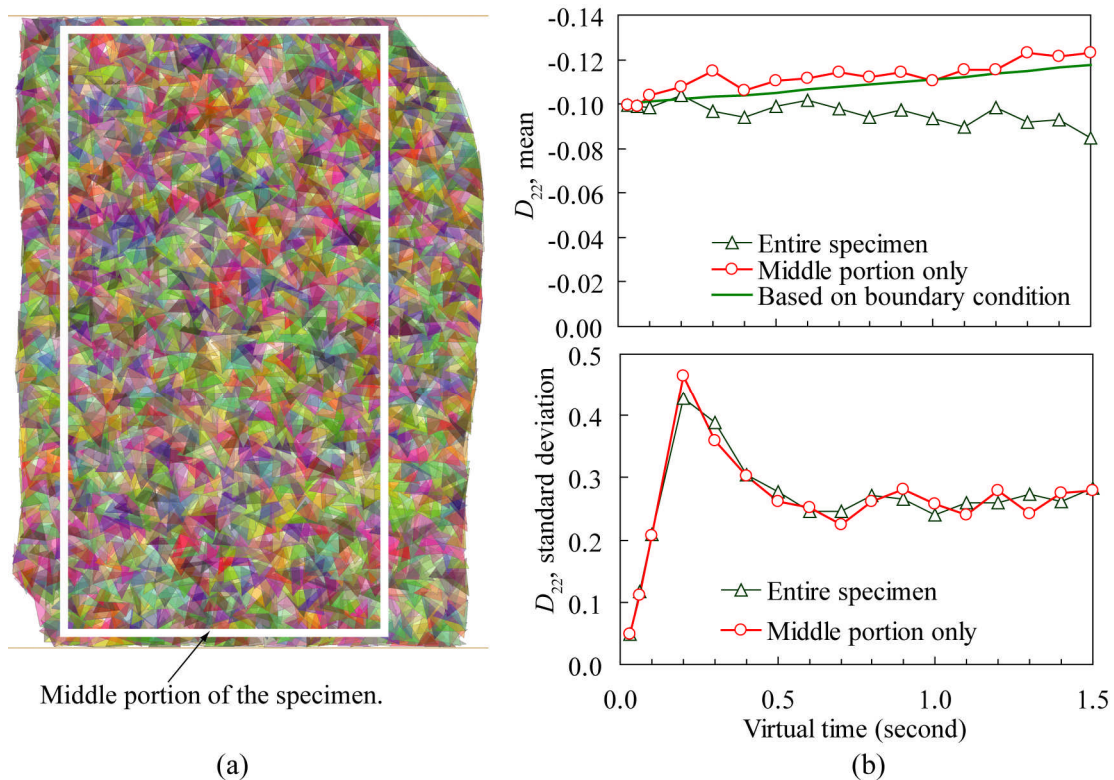


Figure 8 Tracking  $\bar{D}_{22}$  over the simulation. (a) shows the 3,000 overlapping reference triangles (with random semi-transparent colors) and the middle portion of the specimen on which statistical analysis is conducted to avoid the effects of the irregular shape of the left and right boundaries at large deformation; (b) shows the evolution of the mean values and standard deviations of  $D_{22}$  for the entire specimen and the

middle portion.

The mean values of  $D_{22}$  for the middle portion match the calculated rate-of-deformation values based on the boundary condition fairly well, with a clear ascending trend with respect to the virtual time. The difference is reasonably small considering the standard deviations are two to three times of the means. This observation demonstrates the effectiveness of the proposed method. On the other hand, the averages of  $D_{22}$  over the entire specimen have significantly smaller absolute values than those based on the boundary condition. This discrepancy is likely due to the fact that the left and right portions of the specimen near the lateral boundaries are not effectively constrained by the two rigid platens. However, it should be emphasized that both the averages over the entire specimen and that over the middle portion only are valid measurements. Their difference is simply owing to the heterogeneity of the deformation of the specimen, not indicating one is “more correct” than the other.

#### 4. Numerical example II: shear flow and shear banding

The numerical example in Section 3 focuses on the  $D_{22}$  component of the rate-of-deformation tensor, which can be tied to the velocity boundary condition of the simulation. In the current section, we investigate shear flows of the same simulation with an emphasis on the behaviors of shear bands.

##### *4.1 Nucleation of shear bands*

The distribution of  $\dot{\gamma}_{max}$  over the specimen at selected virtual time instants (states ② to ⑦) is shown in Figure 9. Three thousand overlapping reference triangles are randomly placed over the specimen and the average edge length of these triangles is 3 mm. A line segment is drawn at the center of each reference triangle with the length proportional to the magnitude of  $\dot{\gamma}_{max}$  calculated for this reference triangle, and the orientation denoting the maximum local shear flow direction.

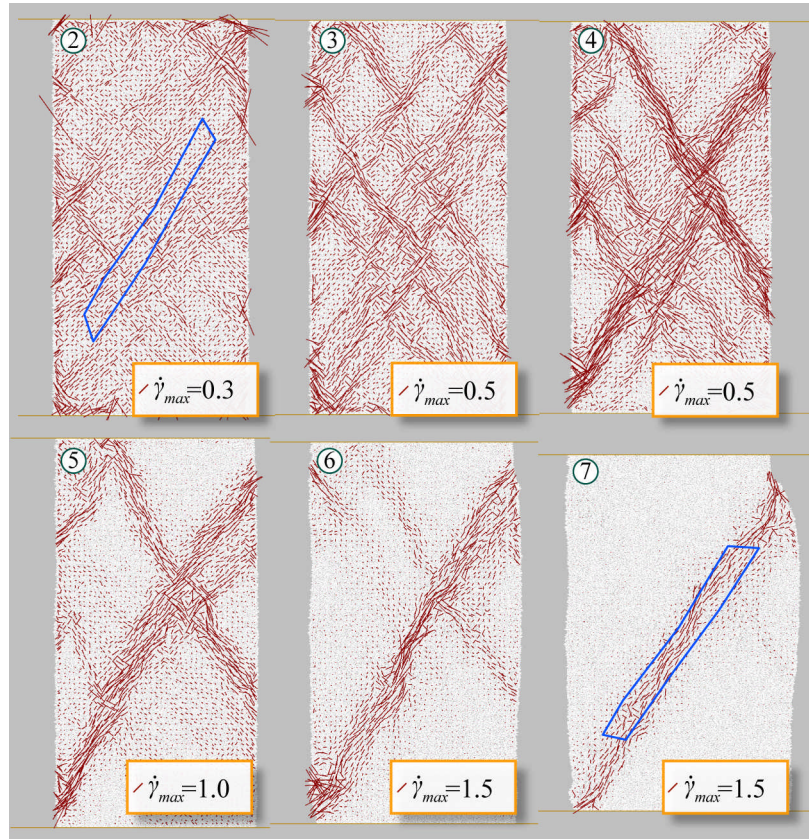


Figure 9 Distribution of  $\dot{\gamma}_{max}$  over the specimen in six selected reference states. Note that the scale of the line segments representing the magnitude of  $\dot{\gamma}_{max}$  varies from one state to another, with the same segment length representing a larger  $\dot{\gamma}_{max}$  value in later states. The blue polygons shown in states ② and ⑦ are “virtual masks” to be used in the analysis of Section 4.2.

The maximum shear flow rate distribution visualized above should be analyzed in conjunction with the following statistical analysis to gain insight into the nucleation process of shear bands. The normalized histogram of the shear flow direction (the angle between the maximum shear flow direction and the horizontal, ranging between 0 and 180°) in each of these states is plotted in Figure 10, which can be used to estimate the probability density function (PDF) of the local shear flow direction. Additionally, the companion normalized histogram *weighted* by the magnitude of  $\dot{\gamma}_{max}$  is also plotted. In weighted histograms, one occurrence of the value  $A$  is equivalent to  $A/B$  occurrences of the value  $B$ . The weighted histogram is potentially a better metric for indicating the dominant direction of local shear flows because it can filter out the unwanted effects of the regions that are not actively deforming. The material in the shear bands is experiencing much higher shear flow rates than the other portions of the specimens and thereby being given higher weights. Note that the statistical analysis is only conducted for the middle portion of the specimen as marked in Figure 8(a) to eliminate the effects of the lateral boundaries. The weighted mean values of the shear flow directions in the intervals of 0° to 90° and 90° to 180° are also calculated separately and marked in the histograms. They help identify the two (applicable to states ② to ⑤) or one (states ⑥ and ⑦) predominant shear flow direction.

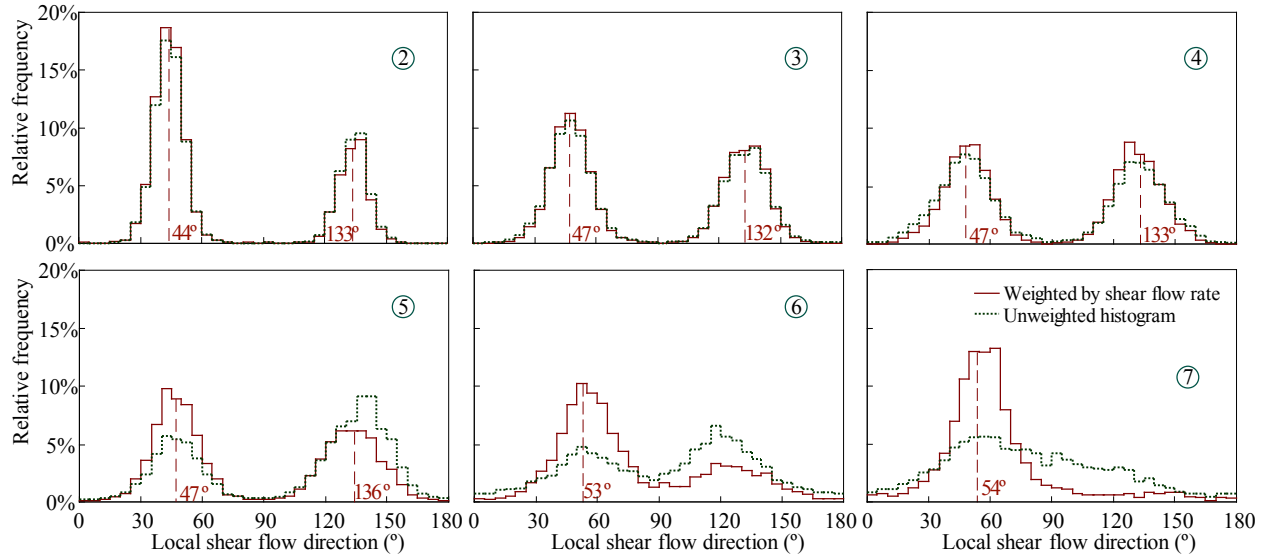


Figure 10 Histograms (weighted and unweighted) of local shear flow directions in six selected states.

In state ② the deformation of the specimen is still in the elastic regime with no apparent localization, so the maximum shear flow rate distributes over the entire specimen rather uniformly. In each sub-domain, the two principal directions of the rate-of-deformation tensor are vertical and horizontal, respectively. The magnitude of the rotation tensor is very small, which is induced by minor inhomogeneity of the deformation. Therefore the calculated predominant shear directions are close to  $45^\circ$  or  $135^\circ$ . Although a considerably larger portion of the specimen shows predominant shear flow directions around  $45^\circ$  than that around  $135^\circ$ , this is likely due to the minor imperfection of the specimen and boundary conditions. In this deformation regime, there is no mechanically significant difference in the deformation patterns between a sub-domain with a shear flow direction of  $45^\circ$  and that with  $135^\circ$ . In states ③ to ⑤, the stress rate is around the peak value. It can be observed in Figure 9 that the deformation starts to show some tendency of concentration in state ③, where three to four parallel bands with concentrated shear flow can be identified in each of the two conjugate directions. In states ④ and ⑤, one shear band gradually gains dominance in each direction. Subsequently at larger deformation, the shear band with an inclination of approximately  $55^\circ$  dictates the deformation, and the shear flow along the conjugate direction diminishes. This process is clearly revealed by both Figure 9 and Figure 10. Although investigating the mechanics behind these interesting phenomena is beyond the scope of this paper, this numerical example clearly visualizes the initiation and nucleation process of the shear bands, providing a promising tool for future investigation. Notice that the definition and measurement of  $\dot{\gamma}_{max}$  is instrumental in plotting the weighted results of Fig. 10.

#### 4.2 Measurements inside shear bands

All the aforementioned analyses have been carried out over the entire specimen. Using the method proposed in this paper, we can also focus the measurement within a specific area such as the shear band. Our previous study of fabric evolution inside shear bands in granular materials with inherent fabric anisotropy has used a preliminary form of the current method, which was proven to be a critical tool to

gain important insight into this problem (Fu and Dafalias, 2011b). In the example shown below, we utilize a “virtual mask”, which is a polygon-shaped area covering the middle portion (to avoid the boundary effects) of the shear band in the steady state, such as shown by blue color in two of the states (② and ⑦) in Figure 9. With its vertices attached to individual particles, the mask can deform with the specimen. Therefore, in the undeformed and elastic states before shear bands have initiated, the mask covers the particles that would form the predominant shear band at a later time. Only the velocity gradient values derived from the reference triangles within the masked area are used in the statistical analysis, and approximately 500 such reference triangles are engaged in this example. The mean maximum shear flow rates  $\dot{\gamma}_{max}$  as well as the standard deviation are shown in Figure 11. The shear flow rates show a clear increasing trend until the steady state is reached, representing the concentration of deformation into the shear band. We have observed in Figure 8 that the standard deviations of  $D_{22}$  for the global measurement are a few times larger than the mean values. This is because the global measurement mixed the results in the shear band where the velocity gradient is very high and those in the remaining portions of the specimen experiencing essentially rigid body motions. On the other hand, the standard deviations of the flow rate within the shear band mask are approximately 40% of the mean values, indicating that the deformation (rate) in the shear band is relatively homogeneous. It is evident that when localized deformation is the dominant mode, the physical and mechanical meanings of globally averaged measurements are rather ambiguous.

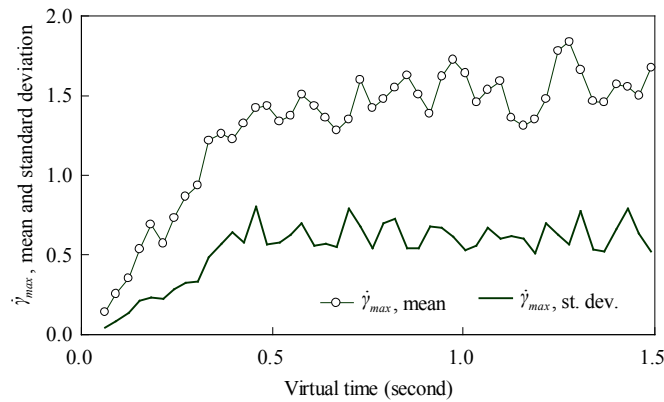


Figure 11 The evolution of shear flow rate in shear band.

### 5. The effects of reference triangle sizes

The analyses in Section 3 and Section 4 have employed reference triangles with an average edge length of 4 mm and 3 mm, respectively. In this section, we evaluate the effects of the sizes of reference triangles, focusing on the  $D_{22}$  measurement in states ② and ⑦ (elastic and steady states, respectively) over the middle portion of the specimen. Four reference triangles sizes with edge lengths of approximately 2, 4, 8, and 16 mm are employed, and on average each of such reference triangles covers a domain consisting of approximately 19, 75, 300, and 1200 particles, respectively. Figure 12 illustrates the sizes of the reference triangles relative to the particle sizes. For each case, a sufficient number of triangles (3,000 to 10,000) are generated to obtain statistically meaningful representations. Additionally, the reference triangles constructed with Delaunay triangulation are the smallest reference triangles that can be adopted, so the Delaunay triangles are included in this evaluation as an extreme scenario. For this specimen with 45,000

particles, the Delaunay triangle system consists of approximately 90,000 triangles, with an average edge length of 0.13 mm.

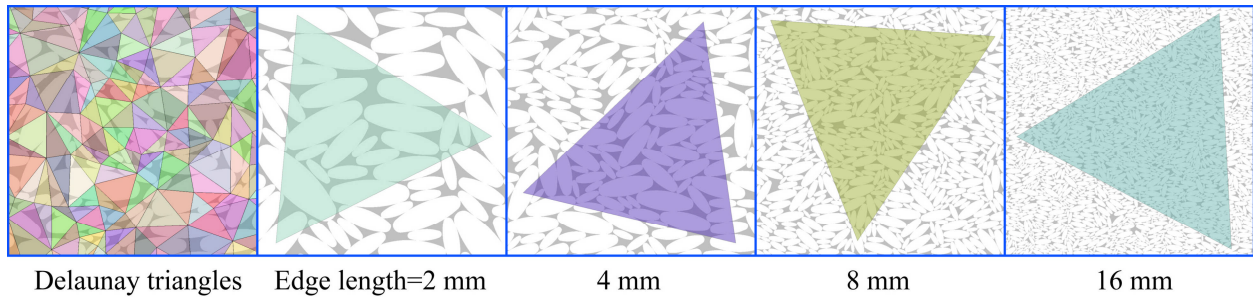


Figure 12 Different reference triangle sizes evaluated.

The mean  $D_{22}$  values as well and the standard deviations in these two states (② and ⑦) are shown in Figure 13 as functions of the reference triangle sizes. In the elastic state, the effects of the reference triangle sizes (including the Delaunay triangles) on the mean value of  $D_{22}$  are observed to be insignificant. The standard deviation increases as the sizes of the triangle decreases. This is intuitive because the results obtained for larger triangles are homogenized measurements for larger domains with more particles, and therefore the random fluctuation of the obtained values should be smaller. It is interesting to notice that while the reference triangle sizes only have a moderate effects on the standard deviation with varying edge lengths between 2mm and 16mm, the standard deviation obtained for the Delaunay triangle system is dramatically larger (by one order of magnitude). Although the aforementioned mechanism (larger domain yields more stable results) should somewhat contribute to this phenomenon, we found that this dramatic discrepancy is primarily attributed to a fundamental difference between the Delaunay triangles and the triangles constructed using the method shown in Figure 1 as elaborated below.

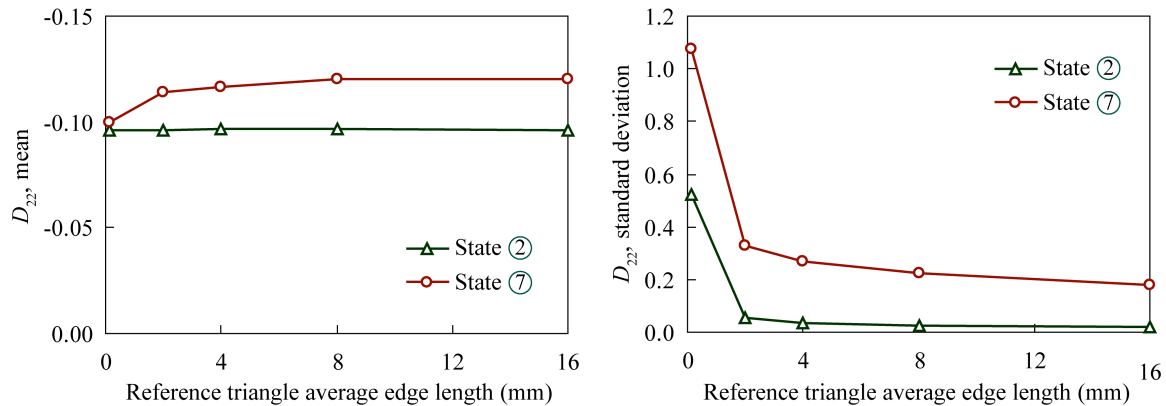


Figure 13 The effects of reference triangle sizes on the rate-of-deformation measurements.

The distributions of  $D_{22}$  in state ② calculated based on reference triangles with 4 mm long edges and the Delaunay triangulation system are shown in Figure 14(a) and (b), respectively. Compared to the relatively uniform distribution of  $D_{22}$  in Figure 14(a), isolated clusters each consisting of a number of relatively

large circular symbols (denoting positive values) and squares (negative values) are the most salient pattern in Figure 14(b). In the magnified view, we can see that at the center of each of these clusters there are one or two kinematically unconstrained small particles. These particles can freely move in the void space between neighboring larger particles, and the magnitude of the displacement is limited by the sizes of the voids but the velocity can be fairly high. Therefore, the velocity gradients obtained from reference triangles attached to these unconstrained particles are often one or two orders of magnitude larger than those from triangles attached to fully constrained particles, and they are considered noises bearing no mechanical significance in representing the deformation of the specimen. The effects of these noises on the mean measurements are likely to be small, since such random velocity of unconstrained particles induces negative velocity gradient values in some reference triangles attached to them while inducing positive values in others. Nevertheless, such noises (orders of magnitude larger than the mean value) are highly undesirable, making the use of the Delaunay triangles as the reference triangles an unappealing option.

A similar investigation is conducted for  $D_{22}$  in state ⑦ and the results included in Figure 13 show similar trends as those for state ②, so they are not further elaborated here. The only exception worth mentioning is that the average magnitude of  $D_{22}$  in state ⑦ calculated based on the Delaunay triangles is perceptibly smaller than the corresponding values based on larger reference triangles. This is likely due to the high noise level and large error margins associated with the Delaunay reference triangles.

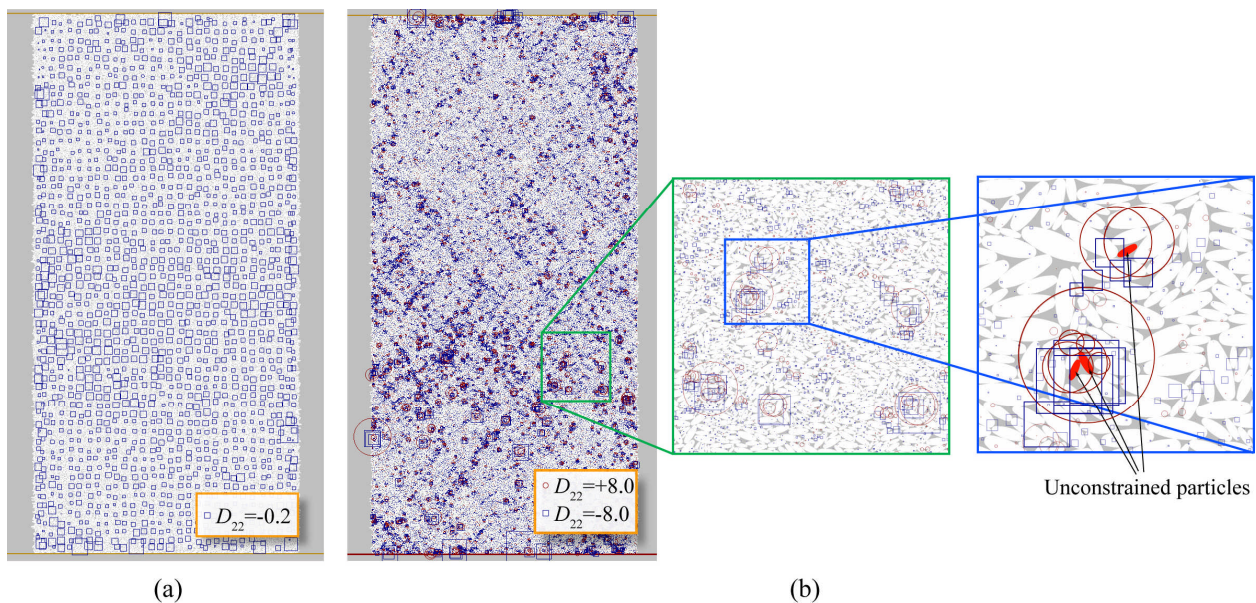


Figure 14 The distribution of  $D_{22}$  calculated based on reference triangles with (a) 4 mm long edges and (b) the Delaunay triangles. Note that positive  $D_{22}$  values are illustrated by circle symbols and negative (in compression) values shown as squares. Also note that the same symbol size in (b) represents 40 times larger  $D_{22}$  values compared to those in (a).

This investigation, although not exhaustive, provides some general guidelines for the selection of reference triangle sizes. If the objective of an analysis is to quantify the homogenized deformation characteristics of a relatively large domain (not necessarily the entire simulation domain or the specimen), the sizes of the reference triangles can be rather freely selected as long as the triangles are significantly smaller than the domain itself. On the other hand, if the distribution patterns of the deformation rate or the integrals over a certain period of time are of interest, the triangles should then be smaller than the desired resolution of the distribution resulting from the analysis. For instance, if we need to investigate the difference between the shear flow rate in a shear band and that in the remainder of the specimen, the edge lengths of the triangles should be smaller than the width of the shear band. Otherwise, the quantified characteristics of the shear band will be smeared by reference triangles covering both the shear band and other parts of the specimen experiencing rigid body displacements. Other important rules that should be observed in generating reference triangles are: 1) larger particles are preferred because they represent the kinematics of the specimen better than smaller particles which are more likely to be kinematically unconstrained; 2) repetitive sampling by using partially overlapping triangles and statistical analysis are encouraged to ensure that the obtained mean values are representative; and 3) the Delaunay triangle systems should be generally avoided because of the significant noises introduced to the results.

## 6. Concluding remarks

In this paper we proposed a new method for quantifying the deformation of granular materials by analyzing movement of individual particles. Two innovations have made the new method more effective and more flexible than the existing methods. First, instead of creating a meshed equivalent continuum attached to the granular particle assembly and assessing the deformation of this continuum, the new method performs independent queries on the deformation characteristics of individual sub-domains, based on which repetitive sampling and statistical analysis convenient. Second, the new formulations are based on the velocity gradient tensor and the rate-of-deformation tensor rather than the more conventional engineering strain. This feature provides a theoretically sound framework for handling large deformation problems, which is essential for investigating behaviors of granular materials where strain localization (or more specifically shear banding) is the most salient mode of failure. Nevertheless, the relationships between the rate-of-deformation measurements and the more conventional strain concepts are explored in the paper.

In the numerical examples presented in this paper, it was first verified that the averaged or homogenized measurements based on the new method are consistent with values estimated on the basis of the imposed boundary conditions. More importantly, we demonstrated how to use the new method to quantify the evolution of deformation rates distributed throughout the specimen, with a special emphasis on the initiation and nucleation of shear bands. Finally, the effects of the sizes of the reference triangles were investigated in order to provide general guidelines for the selection of the reference triangle sizes. An interesting and inspiring finding in this evaluation was that if the Delaunay triangles (or other comparable tessellation methods) are used as the reference triangles, which is a fairly common practice in most existing methods, very significant noises are expected to be introduced into the measurements, which could be detrimental to the statistical interpretation of the results. Therefore, the Delaunay triangulation or similar methods constructing cell systems unselectively based on all particles is not a recommended

approach for constructing reference triangles. This phenomenon has not been mentioned in the literature possibly because most previous studies have used particles of similar sizes, for which this effect is not apparent. This issue has to be dealt with carefully if the granular assembly involves particles with a wide spectrum of particle sizes.

#### Acknowledgments

Pengcheng Fu's work in this paper was partly performed under the auspices of the U.S. Department of Energy by Lawrence Livermore National Laboratory under Contract DE-AC52-07NA27344. Yannis F. Dafalias acknowledges partial support from the European Research Council under the European Community's Seventh Framework Program (FP7/2007-2013) / ERC grant agreement no. 228051. This document has been released with a release number: LLNL-JRNL-479880.

#### References:

- Alshibli, K.A., Sture, S., 1999. Sand shear band thickness measurements by digital image technique. *J. Comput. Civil Eng.* 12(2), 103-109.
- Bagi, K., 1996. Stress and strain in granular assemblies. *Mech. Mater.* 22(3), 165-177, doi: 10.1016/0167-6636(95)00044-5.
- Bagi, K., 2006. Analysis of microstructural strain tensors for granular assemblies. *Int. J. Solids Struct.* 43(10), 3166-3184, doi: 10.1016/j.ijsolstr.2005.07.016.
- Cambou, B., Chaze, M., Dedecker, F., 2000. Change of scale in granular materials. *Eur. J. Mech. A. Solids.* 19(6), 999-1014, doi: 10.1016/S0997-7538(00)01114-1.
- Desrues, J., Chambon, R., Mokni, M., Mazerolle, F., 1996. Void ratio evolution inside shear bands in triaxial sand specimens studied by computed tomography. *Géotechnique* 46(3), 529-546, doi: 10.1680/geot.1996.46.3.529.
- Desrues, J., Viggiani, G., 2004. Strain localization in sand: an overview of the experimental results obtained in Grenoble using stereophotogrammetry. *International Journal for Numerical and Analytical Methods in Geomechanics* 28(4), 279–321. doi: 10.1002/nag.338.
- Durán, O., Kruyt, N., Luding, S., 2010. Analysis of three-dimensional micro-mechanical strain formulations for granular materials: evaluation of accuracy. *Int. J. Solids Struct.* 47(2), 251-260, doi: 10.1016/j.ijsolstr.2009.09.035.
- Finno, R.J., Harris, W.W., Mooney, M.A., Viggiani, G., 1996. Strain localization and undrained steady state of sand. *J. Geotech. Eng.* 12(6), 462-473.
- Finno, R.J., Harris, W.W., Mooney, M.A., Viggiani, G. 1997. Shear bands in plane strain compression of loose sand. *Géotechnique* 47(1), 149-165.
- Fu, P., Dafalias, Y.F., 2011a. Study of anisotropic shear strength of granular materials using DEM

- simulation. *Int. J. Numer. Anal. Methods Geomech.* doi: 10.1002/nag.945.
- Fu, P., Dafalias, Y.F., 2011b. Fabric evolution within shear bands of granular materials and its relation to critical state theory. *Int. J. Numer. Anal. Methods Geomech.* doi: 10.1002/nag.988.
- Fu, P., Walton, O.R., Harvey, J.T., 2011c. Polyarc discrete element for efficiently simulating arbitrarily shaped 2D particles. *Int. J. Numer. Meth. Eng.*, accepted for publication.
- Hall, S.A., Bornert, M., Desrues, J., Pannier, Y., Lenoir, N., Viggiani, G., B  uelle, P., 2010. Discrete and continuum analysis of localised deformation in sand using X-ray  $\mu$ CT and volumetric digital image correlation. *G  otechnique* 60(5), 315-322.
- Hasan, A., Alshibli, K.A., 2010. Experimental assessment of 3D particle-to-particle interaction within sheared sand using synchrotron microtomography. *G  otechnique* 60(5), 369-379.
- ITASCA, 1999. Particle flow code in two dimensions. Users Manual: Theory and Background. ITASCA, Minneapolis, MN, pp. 3.11–3.13.
- Kuhn, M.R., 1999. Structured deformation in granular materials. *Mech. Mater.* 31, 407-429.
- Kruyt, N.P., Rothenburg, L., 1996. Micromechanical definition of the strain tensor for granular materials. *J. Appl. Mech.* 63(3), 706-711, doi: 10.1115/1.2823353.
- Kruyt, N.P., 2003. Statics and kinematics of discrete Cosserat-type granular materials. *Int. J. Solids Struct.* 40(3), 511-534, doi: 10.1016/S0020-7683(02)00624-8.
- Li, X., Li, X.S., 2009. Micro-macro quantification of the internal structure of granular materials. *J. Eng. Mech.* 135(7), 641-656.
- Liao, C., 1997. Stress-strain relationship for granular materials based on the hypothesis of best fit. *Int. J. Solids Struct.* 34(31-32), 4087-4100, doi: 10.1016/S0020-7683(97)00015-2.
- Malvern, L.E., 1969. *Introduction to the Mechanics of a Continuous Medium*. Prentice Hall, Englewood Cliffs, New Jersey.
- M  hlhaus, H.B., Vardoulakis, I., 1987. The thickness of shear bands in granular materials. *G  otechnique* 37(3), 271-283.
- Oda, M., Kazama, H., 1998. Microstructure of shear bands and its relation to the mechanisms of dilatancy and failure of dense granular soils. *G  otechnique* 48(4), 465-481.
- Rechenmacher, A.L., 2006. Grain-scale processes governing shear band initiation and evolution in sands. *Journal of the Mechanics and Physics of Solids*, 54(1):22–45. DOI: 10.1016/j.jmps.2005.08.009.
- Tordesillas, M., Walsh, S.D.C., Muthuswamy M., 2008. The Effect of local kinematics on the local and global deformations of granular systems. *Mathematics and Mechanics of Solids*, 15(1): 3-41, doi: 10.1177/1081286508089844.
- Vermeer, P.A., 1990. The orientation of shear bands in biaxial tests. *Geotechnique*; 40(2):223–236.